THE JOURNAL OF PHYSICAL CHEMISTRY Letters

LETTER

pubs.acs.org/JPCL

$SrTiO_3$ Nanotubes with Negative Strain Energy Predicted from First Principles

Sergei Piskunov*,† and Eckhard Spohr‡

†Faculty of Computing, University of Latvia, 19 Raina Blvd., Riga LV-1586, Latvia, Faculty of Physics and Mathematics, University of Latvia, 8 Zellu Str., Riga LV-1002, Latvia, and Institute for Solid State Physics, University of Latvia, 8 Kengaraga Str., Riga LV-1063, Latvia

‡Department of Theoretical Chemistry, University of Duisburg-Essen, Universitätstr. 2, D-45141 Essen, Germany

ABSTRACT: On the basis of hybrid density functional theory calculations, we predict that the most energetically favorable single-walled $SrTiO_3$ nanotubes with negative strain energy can be folded from $SrTiO_3$ (110) nanosheets of rectangular morphology. Further formation of multiwalled tubular nanostructure with interwall distance of ∼0.46 nm yields an additional gain in energy of 0.013 eV per formula unit. (The formation energy of the most stable nanotube is 1.36 eV/$SrTiO_3$.) Because of increase in the Ti−O bond covalency in the outer shells, $SrTiO_3$ nanotubes can demonstrate an enhancement of their adsorption properties. Quantum confinement leads to a widening of the energy band gap of single-walled $SrTiO_3$ nanotubes (∼6.1 eV) relative to the bulk (∼3.6 eV), which makes them attractive for further band gap engineering.

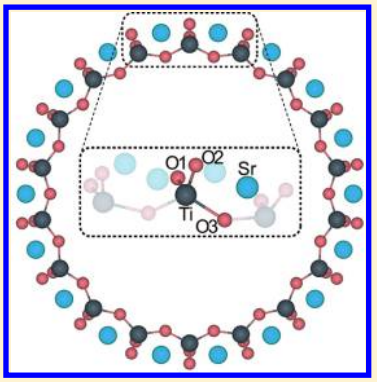

SECTION: Nanoparticles and Nanostructures

One-dimensional (1D) nanostructures made from complex ternary oxides with a perovskite structure have attracted considerable recent interest because of their unique physical properties and promising novel functionalities compared with bulk materials.[1,2] Among them, strontium titanate nanotubes (hereafter NTs) are proposed as comaterials for high-performance photoelectrochemical TiO_2 electrodes to be used in dye-sensitized solar cells or for photocatalytic hydrogen production[3,4] and even as a Sr delivery platform on osteoporotic Ti-based bone implants.[5] At room-temperature, $SrTiO_3$ possesses a high symmetry cubic structure and thus serves as an excellent model material for a wide class of ABO_3 perovskites. Consequently, understanding the behavior of $SrTiO_3$ on the nanoscale is significant for fundamental studies as well as for shape-controlled synthesis of perovskite nanostructures with predictable properties.

Recently, intense experimental efforts have been made in preparation of perovskite nanotubes via the low-temperature hydrothermal reaction route using simple oxide nanotubes as a precursor. (See ref 2 and references therein.) Typical ABO_3 perovskites are nonlayered compounds and thus tend to form polycrystalline nanotubes composed of nanosized perovskite crystallites.[6] Nevertheless, recent transmission electron microscopy and electron diffraction observations indicate that monocrystalline perovskite nanotubes can be synthesized.[7,8] In fact, monophasic NTs having an inner diameter from 4 to 7 nm, outer diameter from 8 to 15 nm, and a length from 50 to over 500 nm have been reported.[9] Recent first-principles studies provide valuable insight into the behavior of 1D ABO_3 nanowires emphasizing their size-dependent ferroelectric properties (see, e.g., refs 10−12). Interestingly, results of ab initio simulations performed on ABO_3 nanotubes are very scarce in the literature.

The purpose of this Letter is to predict from first principles the atomic and electronic structure of the energetically most stable monocrystalline NTs folded from 2D $SrTiO_3$ nanosheets (hereafter NSes). To perform calculations, we used the density functional theory/Hartree−Fock hybrid exchange-correlation technique, which was shown to yield reliable results for the electronic and atomic structure both for bulk $SrTiO_3$[13] and its low-index surfaces.[14] We employ the hybrid B3PW exchange-correlation functional consisting of the nonlocal HF exchange, DFT exchange, and generalized gradient approximation (GGA) correlation functionals as proposed by Becke.[15] The calculations were carried out with the CRYSTAL computer code,[16] with atom-centered Gaussian-type functions as basis set (BS). BSs for Sr, Ti, and O have been taken from ref 13. Reciprocal space integration was performed by sampling the Brillouin zone with the 8 × 8 × 1 and 8 × 1 × 1 Pack−Monkhorst mesh[17] for 2D NSes and 1D NTs, respectively. To obtain equilibrium structures, we allowed the lattice constants and all atoms in the NS and NT unit cells to relax. The effective charges on atoms as well as net bond populations have been calculated according to the Mulliken population analysis.[16]

Studied NTs are modeled using layer folding approach, which means the formation builds of cylindrical NT structure by rolling up the stoichiometric 2D NS cut from $SrTiO_3$ bulk parallel to

Received: August 2, 2011
Accepted: September 23, 2011

   dx.doi.org/10.1021/jz201050e | J. Phys. Chem. Lett. 2011, 2, 2566–2570

Table 1. Equilibrium Lattice Constants (a_0 and b_0 in nanometers), Thickness (d^{NS} in nanometers), Formation Energy with Respect to the Bulk (E^{NS}_{form} in eV/$SrTiO_3$), and Band Gaps (δ in electronvolts) of NSes under Study[a]

$SrTiO_3$	lattice	a_0	b_0	d^{NS}	E^{NS}_{form}	δ
SL-(001)-NS	square	0.385		0.197	1.84	3.63
DL-(001)-NS	square	0.386		0.591	1.10	2.58
SL-(110)-NS	rectangular	0.353	0.593	0.204	1.81	5.98
DL-(110)-NS	rectangular	0.359	0.588	0.583	1.41	5.40
SL-(111)-NS	barrierless reconstruction to SL-(110)-NS					
DL-(111)-NS	hexagonal	0.582		0.289	2.83	4.15
bulk	cubic	0.391				3.64
bulk (exptl)	cubic	0.390[18]				3.25[19]

[a] Symmetry constraints were removed. Last two rows contain data for $SrTiO_3$ bulk. Abbreviation, e.g., SL-(001)-NS means that it is single-layered (SL) $SrTiO_3$ nanosheet (NS) cut parallel to (001) surface of cubic $SrTiO_3$.

either (001) or (110) or (111) surfaces. Within the framework of our current study, we considered single-layered (SL) and double-layered (DL) NSes (and NTs) consisting of two or four alternating SrO- and TiO_2-(001), SrTiO- and O_2-(110), and SrO_3 - and Ti-(111) atomic surfaces planes, respectively. In the CRYSTAL calculations, the 1D NTs are modeled employing solely their helical rototranslational symmetry;[16] for the 2D NSes, only the translational symmetry operator has been employed.

Table 1 lists equilibrium lattice parameters, formation energies, and band gaps (δ) as calculated for NSes under study. The NS formation energies per $SrTiO_3$ formula unit are defined as $E^{NS}_{form} = E^{NS}_{tot}/m - E^{bulk}_{tot}$, where E^{NS}_{tot} is the total energy of relaxed NS consisting of m bulk formula units and E^{bulk}_{tot} is the total energy calculated for $SrTiO_3$ bulk. Lattice parameters of NSes are slightly reduced with respect to the bulk. Because of quantum confinement δ of (110)- and (111)-NSes increases with respect to the bulk, while decrease of δ is obtained for (001)-NS due to surface effect.[14] Of peculiar interest is DL-(110)-NS, which after geometry optimization performed without symmetry constraints reveals a quasi-layered 2D structure (see Figure 1) with relatively low NS formation energy. Similar quasi-layered 2D nanostructures were also obtained for triple- and four-layered (110)-NS. This makes it probable that the formation of NTs by folding SL-(110)-NS may require less energy with respect to (001)- and (111)-NSes. Note that SL-(111)-NS during geometry optimization experiences barrierless (spontaneous) reconstruction to SL-(110)-NS. E^{NS}_{form} calculated for DL-(111)-NS is more than two times larger than for DL-(001)-NS and DL-(110)-NS, implying that DL-(111)-NS is less attractive for the study of NT formation. We thus only consider NTs folded from the energetically most favorable SL and DL (001)- and (110)-NSes of square and rectangular lattices, respectively.

The orthogonality of the chiral and the translation vectors makes possible the formation of NTs with (n_1,n_2) chirality if folded from a nanosheet with a square 2D lattice (n_1 and n_2 are any integer), whereas only $(n_1,0)$ or $(0,n_1)$ chirality is possible for NTs with rectangular morphology. (See refs 20−22 for a thorough discussion.) In this Letter, we consider NTs $(n,0)$ and (n,n) if they are rolled up from (001)-NSes and NTs $(n,0)$ and $(0,n)$ rolled up from (110)-NSes. In the current version of the CRYSTAL code, the number of symmetry operators is limited to 48. Therefore, the maximum possible chirality index is $n = 24$ for (001)-NTs (n,n) and $n = 48$ for the (001)-NTs $(n,0)$ and for all (110)-NTs. NTs with higher chirality number can be calculated by, for example, doubling the 2D NS unit cell in the corresponding directions, but such CPU-intensive calculations were not within the scope of this manuscript. Depending on the choice of the inner shell, two NTs of the same chirality rolled up from the same NS are possible; for example, NT (48,0) folded from SL-(110)-NS with SrTiO-terminated inner shell [SL-SrTiO-(110)-NT (48,0)] and NT (48,0) folded from SL-(110)-NS with O_2-terminated inner shell [SL-O_2-(110)-NT (48,0)] are two different NTs. The termination of the outer shell of each NT is defined by the stacking sequence of corresponding NS.

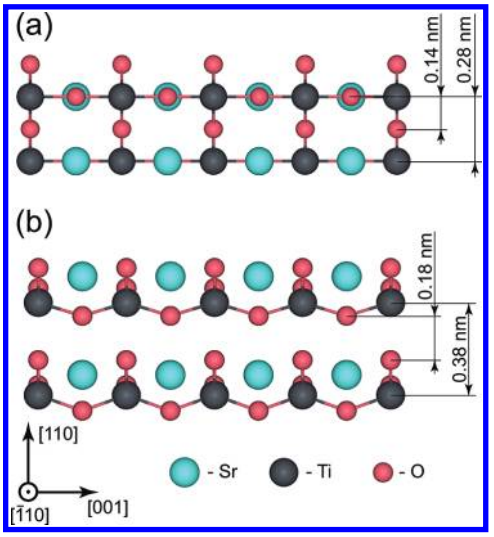

Figure 1. Schematic representation of DL-(110)-NS: (a) as cut from the bulk and (b) after full atomic relaxation without symmetry constraints.

Taking into account the fact that the asymmetry of the structure of the two sides of slab layer is one of the driving forces for the folding of NS into NT and because the strain originating from the curvature of the NT is expected to play a major role in the NT formation process, we assume that the energetically most stable NT should possess both a negative strain energy ($E_{strain} = E^{NT}_{tot}/k - E^{NS}_{tot}/m$, where E^{NT}_{tot} is the total energy of relaxed NT consisting of k bulk formula units), indicating stability of the NT relative to the corresponding flat NS and the lowest NT formation energy with respect to the bulk: $E^{NT}_{form} = E^{NS}_{form} + E_{strain}$, where E^{NS}_{form} is the energy required to cut corresponding NS from the bulk. We note that these energies are calculated from the total electronic energies and further inclusion of vibrational contributions may unsubstantially affect the energy of formation.

According to our calculations (Figure 2 and Table 2), the above-mentioned condition is fulfilled for SL-SrTiO-(110)-NTs $(n,0)$ beginning with $n = 7$ (inner diameter $D = 0.68$ nm). Negative strain energies are also predicted for SL-O_2-(110)-NTs $(0,n)$ beginning with $n = 8$ ($D = 1.3$ nm); however, their formation energies are larger with respect to those calculated for SL-SrTiO-(110)-NTs $(n,0)$. The presence of a minimum in the E_{strain} curve of SL-SrTiO-(110)-NTs $(n,0)$ (Figure 2) suggests a preference for NTs of $D \approx 1.5$ nm; however, no experimental evidence is reported to date.

The smallest negative E_{strain} of −0.02 eV/$SrTiO_3$ for DL-NTs has been calculated for DL-SrTiO-(110)-NT (48,0) ($D = 4.98$ nm).

dx.doi.org/10.1021/jz201050e |J. Phys. Chem. Lett. 2011, 2, 2566–2570

However, in the case of DL-NTs E_{strain} rises quickly as the inner diameter D decreases: for example, DL-SrTiO-(110)-NT (40,0) (D = 4.42 nm) already yields a positive value of E_{strain}. Also, all NTs folded from the (001)-NS have positive strain energies. (See Table 2.) Therefore, we can predict that NTs of inner diameter <4.4 nm consist of shells rolled up from SL-(110)-NS, whereas NTs of larger D can possibly also be folded from DL-(110)-NS. Note that negative E_{strain} minimizes the NT formation energy with respect to the $SrTiO_3$ bulk (Table 2 for E^{NT}_{form}); nevertheless, the latter remains relatively high. For instance, the most energetically stable SL-SrTiO-(110)-NT (18,0) has E_{strain} of −0.455 eV/$SrTiO_3$ or −0.091 eV/atom, which is smaller compared with the negative strain energies predicted for zigzag imogolite nanotube, E_{strain} = −0.038 eV/atom,[23] or for three-monolayer anatase (001) nanotube, E_{strain} = −0.053 eV/atom,[24] but the E^{NT}_{form} calculated for SL-SrTiO-(110)-NT (18,0) is nearly two times larger than that predicted for three-monolayer anatase (001) nanotube, 0.271 versus 0.133 eV/atom.[24]

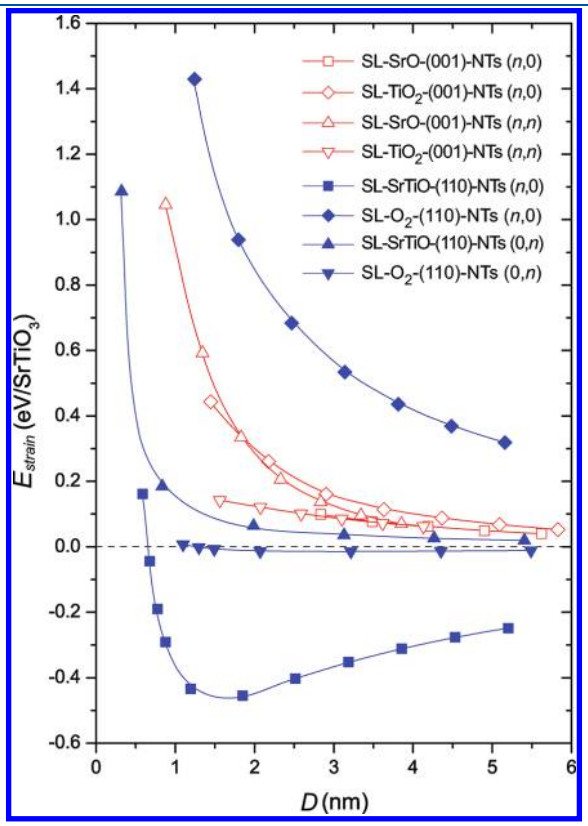

Figure 2. Calculated strain energies (E_{strain}) of NTs as a function of the nanotube inner diameter (D). Strain energy per $SrTiO_3$ formula unit is defined as the difference between the total energies calculated for the NT and the corresponding flat NS. See Table 2 for abbreviations.

The smallest NTs synthesized in the laboratory possess a wall thickness of ∼4 nm,[9] whereas the SL- and DL-NTs studied here have a thickness of 0.2 and 0.6 nm, respectively. Obviously already the smallest synthetic NTs are multiwalled NT structures; that is, they consist of a number of commensurate NTs embedded into each other. We have calculated the properties of a multiwalled SL-SrTiO-(110)-NT (12,0)@(24,0)@(36,0), which has inner diameter of 1.19 nm, outer diameter of 4.26 nm, and interwall distance of 0.46 nm. This multiwalled structure is indeed stabilized by 0.013 eV/$SrTiO_3$ relative to its NT's constituents. Further optimization of multiwalled NT interwall distance by matching of its NT constituents may result in energetically even more stable NT structure, but this is beyond the scope of the current study.

The projected density of state calculated for the most stable NTs and NSes shows that the top of their valence bands and the bottom of their conduction bands consist of O 2p and Ti 3d orbitals, respectively, as in bulk $SrTiO_3$. However, quantum confinement widens the NT's band gap (Tables 1 and 2).

Table 2. Number of Atoms in the Unit Cell (N), Length of Translation Vector (L in nanometers), Inner Diameter (D in nanometers), Wall Thickness (i.e., Distance between the Most Inner and the Most Outer Atom of NT, d^{NT} in nanometers), Strain Energy (E_{strain} in eV/$SrTiO_3$), Formation Energy with Respect to the Bulk (E^{NT}_{form} in eV/$SrTiO_3$), and Band Gaps (δ in electronvolts) of SL- and DL-NTs with Largest Chirality Numbers As Calculated in the Present Study[a]

	N	L	D	d^{NT}	E_{strain}	E^{NT}_{form}	δ
SL-SrO-(001)-NT (48,0)	240	0.382	5.62	0.201	0.04	1.88	3.85
DL-SrO-(001)-NT (48,0)	480	0.377	5.67	0.577	0.02	1.12	3.90
SL-TiO_2-(001)-NT (48,0)	240	0.387	6.83	0.194	0.05	1.90	3.77
DL-TiO_2-(001)-NT (48,0)	480	0.394	5.10	0.653	0.15	1.26	2.72
SL-SrO-(001)-NT (24,24)	240	0.542	3.85	0.199	0.07	1.91	3.52
DL-SrO-(001)-NT (24,24)	480	0.555	3.72	0.581	0.37	1.47	3.63
SL-TiO_2-(001)-NT (24,24)	240	0.546	4.13	0.193	0.06	1.91	3.79
DL-TiO_2-(001)-NT (24,24)	480	0.553	3.90	0.573	0.38	1.49	3.35
SL-SrTiO-(110)-NT (48,0)	240	0.589	5.20	0.205	−0.25	1.56	6.10
DL-SrTiO-(110)-NT (48,0)	480	0.589	4.98	0.574	−0.02	1.38	5.18
SL-O_2-(110)-NT (48,0)	240	0.599	5.16	0.203	0.32	2.13	5.83
DL-O_2-(110)-NT (48,0)	480	0.615	4.80	0.535	0.45	1.86	4.28
SL-SrTiO-(110)-NT (0,48)	240	0.353	8.80	0.204	0.01	1.82	5.97
DL-SrTiO-(110)-NT (0,48)	480	0.350	8.71	0.557	0.05	1.45	5.27
SL-O_2-(110)-NT (0,48)	240	0.352	8.89	0.205	−0.01	1.80	6.00
DL-O_2-(110)-NT (0,48)	480	0.358	8.23	0.588	−0.01	1.40	5.32

[a] Abbreviation SL-SrO-(001)-NT denotes a $SrTiO_3$ nanotube (NT) folded from single-layered (SL) nanosheet cut parallel to (001) surface of $SrTiO_3$ bulk. NT's inner shell termination is SrO. NT's outer shell termination is therefore TiO_2 (assumed but not included into the abbreviation).

Table 3. Calculated Effective Mulliken Charges (Q in e), Ti−O Bond Lengths (l in nanometers), and Ti−O Bond Populations (P in milli e) of SL-SrTiO-(110)-NT (18,0), SL-(110)-NS, and $SrTiO_3$ Bulk[a]

	Q_{Sr}	Q_{Ti}	Q_{O1}	Q_{O2}	Q_{O3}	l_{Ti-O1}	l_{Ti-O2}	l_{Ti-O3}	P_{Ti-O1}	P_{Ti-O2}	P_{Ti-O3}
SL-SrTiO-(110)-NT	1.85	2.22	−1.40	−1.34	−1.32	0.178	0.177	0.188	138	136	106
SL-(110)-NS	1.83	2.22	−1.38	−1.31	−1.37	0.177	0.176	0.195	156	150	102
bulk	1.87	2.35	−1.41	−1.41	−1.41	0.196	0.196	0.196	88	88	88

[a] See Figure 3 for notations.

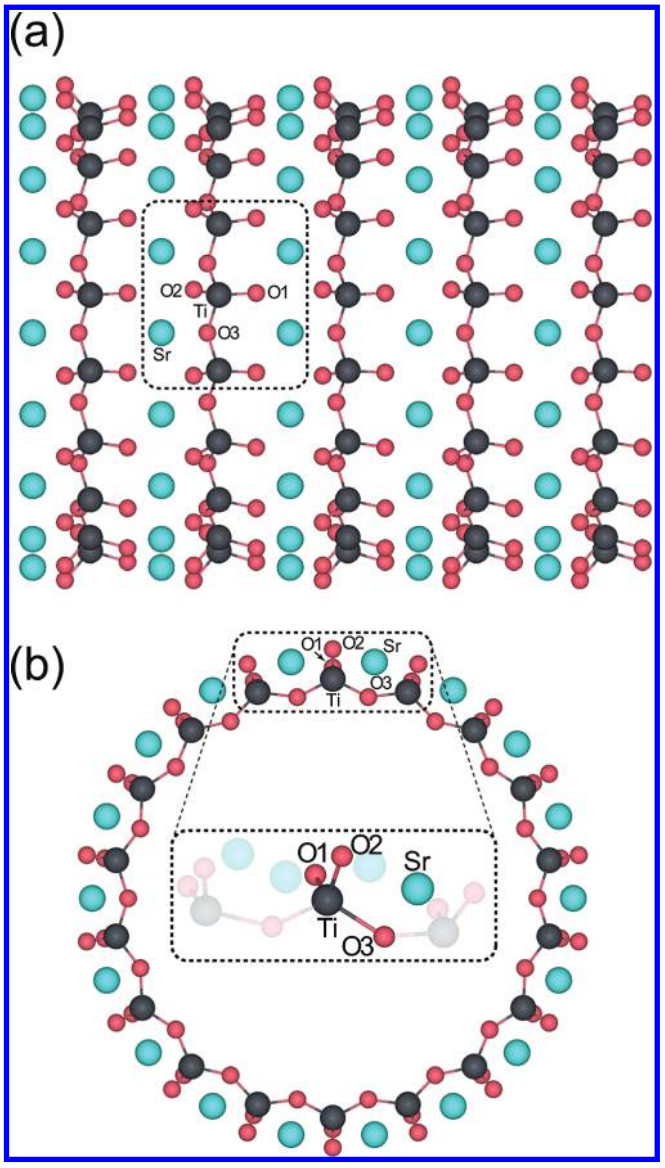

Figure 3. Side view (a) and front view (b) of SL-SrTiO-(110)-NT (18,0). Unshaded area of inset depicts irreducible atoms of nanotube unit cell. See Table 2 for abbreviations.

(The band gap becomes smaller as the number of atoms in NT unit cell increases, e.g., SL-SrTiO-(110)-NT (48,0), δ = 6.10 eV; DL-SrTiO-(110)-NT (48,0), δ = 5.18 eV; SL-SrTiO-(110)-NT (12,0)@(24,0)@(36,0), δ = 3.72 eV; and $SrTiO_3$ bulk, δ = 3.64 eV.) Doping of NTs may lead to the formation of defect states in the band gap, and thus the wider band gap provides additional freedom for band gap engineering. Note that because of the combined effects of NT curvature and of carrier confinement in the NT shell, the excitonic binding energy might be substantially stronger than in the bulk and thus might play a crucial role in various optoelectronic applications.

Table 3 lists effective Mulliken charges, Ti−O bond lengths, and Ti−O bond populations calculated for SL-SrTiO-(110)-NT (18,0), SL-(110)-NS, and $SrTiO_3$ bulk. Significant reconstruction of the NSes results in the breaking of a Ti−O bond from the perovskite oxygen octahedron. (See Figures 1 and 3.) This leads to the formation of considerably shorter Ti−O1 and Ti−O2 bonds accompanied by a change of effective charges and a covalency (bond population) increase relative to the bulk for both the (110)-NS and the outer shell of corresponding NTs. O1 and O2 oxygen atoms in the outer shell of SL-SrTiO-(110)-NT (n,0) may be able to form strong bonds with, for example, adsorbed molecular oxygen by forming surface molecular peroxide.[25,26]

In summary, on the basis of ab initio calculation, we predict that the most energetically stable NTs can be rolled up from (110)-NS of rectangular morphology. Because $SrTiO_3$ is a model material for many pseudocubic perovskites, we suggest that NTs with the rectangular morphology be produced from other ABO_3 perovskites. The increase of the Ti−O bond covalency in the outer NT shell may lead to an enhancement of adsorption properties. This would imply that NTs can be used in gas-sensing devices. Quantum confinement effects lead to the widening of the NT band gaps and makes them thus attractive for band gap engineering in, for example, photocatalytic applications.

AUTHOR INFORMATION

Corresponding Author
*E-mail: piskunov@lu.lv.

ACKNOWLEDGMENT

This work was supported by the Alexander von Humboldt Foundation. S.P. is also thankful for the financial support through the ESF project no. 2009/0216/1DP/1.1.1.2.0/09/APIA/VIAA/044. We thank R. A. Evarestov and Yu. F. Zhukovskii for many fruitful discussions.

REFERENCES

(1) Zhu, X.; Liu, Z.; Ming, N. Perovskite Oxide Nanowires: Synthesis, Property and Structural Characterization. *J. Nanosci. Nanotechnol.* **2010**, *10*, 4109–4123.

(2) Zhu, X.; Liu, Z.; Ming, N. Perovskite Oxide Nanotubes: Synthesis, Structural Characterization, Properties and Applications. *J. Mater. Chem.* **2010**, *20*, 4015–4030.

(3) Zhang, X.; Huo, K.; Hu, L.; Wu, Z.; Chu, P. K. Synthesis and Photocatalytic Activity of Highly Ordered TiO_2 and ($SrTiO_3$/TiO_2) Nanotube Arrays on Ti Substrates. *J. Am. Ceram. Soc.* **2010**, *93*, 2771–2778.

(4) Zhang, J.; Bang, J. H.; Tang, C.; Kamat, P. V. Tailored TiO_2–$SrTiO_3$ Heterostructure Nanotube Arrays for Improved Photoelectrochemical Performance. *ACS Nano* **2010**, *4*, 387–395.

(5) Xin, Y.; Jiang, J.; Huo, K.; Hu, T.; Chu, P. K. Bioactive $SrTiO_3$ Nanotube Arrays: Strontium Delivery Platform on Ti-Based Osteoporotic Bone Implants. *ACS Nano* **2009**, *3*, 3228–3234.

(6) Kim, J.; Yang, S. A.; Choi, Y. C.; Han, J. K.; Jeong, K. O.; Yun, Y. J.; Kim, D. J.; Yang, S. M.; Yoon, D.; Cheong, H.; Chang, K.-S.; Noh, T. W.; Bu, S. D. Ferroelectricity in Highly Ordered Arrays of Ultra-Thin-Walled $Pb(Zr,Ti)O_3$ Nanotubes Composed of Nanometer-Sized Perovskite Crystallites. *Nano Lett.* **2008**, *8*, 1813–1818.

(7) Yang, Y.; Wang, X.; Zhong, C.; Sun, C.; Li, L. Ferroelectric $PbTiO_3$ Nanotube Arrays Synthesized by Hydrothermal Method. *Appl. Phys. Lett.* **2008**, *92*, 122907.

(8) Yang, Y.; Wang, X.; Sun, C.; Li, L. Structure Study of Single Crystal $BaTiO_3$ Nanotube Arrays Produced by the Hydrothermal Method. *Nanotechnology* **2009**, *20*, 055709.

(9) Mao, Y.; Banerjee, S.; Wong, S. Hydrothermal Synthesis of Perovskite Nanotubes. *Chem. Commun.* **2003**, *2003*, 408–409.

(10) Geneste, G.; Bousquet, E.; Junquera, J.; Ghosez, P. Finite-Size Effects in $BaTiO_3$ Nanowires. *Appl. Phys. Lett.* **2006**, *88*, 112906.

(11) Shimada, T.; Tomoda, S.; Kitamura, T. Ab Initio Study of Ferroelectricity in Edged $PbTiO_3$ Nanowires Under Axial Tension. *Phys. Rev. B* **2009**, *79*, 024102.

(12) Hong, J.; Catalan, G.; Fang, D. N.; Artacho, E.; Scott, J. F. Topology of the Polarization Field in Ferroelectric Nanowires from First Principles. *Phys. Rev. B* **2010**, *81*, 172101.

(13) Piskunov, S.; Heifets, E.; Eglitis, R. I.; Borstel, G. Bulk Properties and Electronic Structure of $SrTiO_3$, $BaTiO_3$, $PbTiO_3$ Perovskites: An *ab initio* HF/DFT Study. *Comput. Mater. Sci.* **2004**, *29*, 165–178.

(14) Piskunov, S.; Kotomin, E. A.; Heifets, E.; Maier, J.; Eglitis, R. I.; Borstel, G. Hybrid DFT Calculations of the Atomic and Electronic Structure for ABO_3 Perovskite (001) Surfaces. *Surf. Sci.* **2005**, *575*, 75–88.

(15) Becke, A. D. Density-Functional Thermochemistry. III. The Role of Exact Exchange. *J. Chem. Phys.* **1993**, *98*, 5648–5652.

(16) Dovesi, R.; Saunders, V. R.; Roetti, C.; Orlando, R.; Zicovich-Wilson, C. M.; Pascale, F.; Civalleri, B.; Doll, K.; Harrison, N. M.; Bush, I. J.; D'Arco, Ph.; Llunell, M. *CRYSTAL09 User's Manual*; University of Torino: Torino, Italy, 2009. http://www.crystal.unito.it/ (accessed Aug 1, 2011).

(17) Monkhorst, H. J.; Pack, J. D. Special Points for Brillouin-Zone Integrations. *Phys. Rev. B* **1976**, *13*, 5188–5192.

(18) Abramov, Y. A.; Tsirelson, V. G.; Zavodnik, V. E.; Ivanov, S. A.; Brown, I. D. The Chemical Bond and Atomic Displacements in $SrTiO_3$ from X-Ray Diffraction Analysis. *Acta Cryst. B* **1995**, *51*, 942–951.

(19) van Benthem, K.; Elsässer, C.; French, R. H. Bulk Electronic Structure of $SrTiO_3$: Experiment and Theory. *J. Appl. Phys.* **2001**, *90*, 6156–6164.

(20) Enyashin, A. N.; Seifert, G. Structure, Stability and Electronic Properties of TiO_2 Nanostructures. *Phys. Status Solidi B* **2005**, *242*, 1361–1370.

(21) Chernozatonskii, L.; Sorokin, P.; Fedorov, A. Energy and Electronic Properties of Non-Carbon Nanotubes Based on Silicon Dioxide. *Phys. Solid State* **2006**, *48*, 2021–2027.

(22) Evarestov, R.; Bandura, A.; Losev, M.; Piskunov, S.; Zhukovskii, Y. Titania Nanotubes Modeled From 3- and 6-Layered (101) Anatase Sheets: Line Group Symmetry and Comparative Ab Initio LCAO Calculations. *Physica E* **2010**, *43*, 266–278.

(23) Guimarães, L.; Enyashin, A. N.; Frenzel, J.; Heine, T.; Duarte, H. A.; Seifert, G. Imogolite Nanotubes: Stability, Electronic, and Mechanical Properties. *ACS Nano* **2007**, *1*, 362–368.

(24) Ferrari, A. M.; Szieberth, D.; Zicovich-Wilson, C. M.; Demichelis, R. Anatase(001) 3 ML Nanotubes, The First TiO_2 Nanotube With Negative Strain Energies: A DFT Prediction. *J. Phys. Chem. Lett.* **2010**, *1*, 2854–2857.

(25) Piskunov, S.; Zhukovskii, Y. F.; Kotomin, E. A.; Heifets, E.; Ellis, D. E. Adsorption of Atomic and Molecular Oxygen on the SrTiO3(001) Surfaces: Predictions by Means of Hybrid Density Functional Calculations. *Mater. Res. Soc. Symp. Proc.* **2006**, *894*, LL08.05.

(26) Alexandrov, V.; Piskunov, S.; Zhukovskii, Y. F.; Kotomin, E. A.; Maier, J. First-Principles Modeling of Oxygen Interaction with SrTiO3-(001) Surface: Comparative Density-Functional LCAO and Plane-Wave Study. *Integr. Ferroelectr.* **2011**, *123*, 10–17.